Advances in Bridge Engineering

ORIGINAL INNOVATION

Open Access

Identification of modal parameters of long-span bridges under various wind velocities

Siying Lu[1], Lei Yan[1,2,3*], Xuhui He[1,2,3] and Hui Guo[4]

*Correspondence:
leiyan@csu.edu.cn

[1] School of Civil Engineering, Central South University, Changsha 410075, China
[2] National Engineering Research Center for High-Speed Railway Construction, Changsha 410075, China
[3] Hunan Provincial Key Laboratory for Disaster Prevention and Mitigation of Rail Transit Engineering Structures, Changsha 410075, China
[4] Railway Engineering Research Institute, China Academy of Railway Sciences, Beijing 100081, China

Abstract

The modal parameters identification of bridges under non-stationary environmental excitation has caught the attention of researchers. This paper studies the non-stationarity of wind velocity, and extracts the time-varying mean wind velocity based on a discrete wavelet transform and recursive quantitative analysis. The calculated turbulence intensity and turbulence integral scale under the non-stationary model are smaller than those under the stationary model, especially the turbulence integral scale. The empirical wavelet transform is used to identify the modal parameters of long-span bridges, and the power spectral density spectrum is proposed as a replacement for the Fourier spectrum as the basis of the frequency band selection. The bridge modal parameters are then compared using the covariance-driven stochastic subspace system identification method (SSI-COV) and the Hilbert transform method based on an improved empirical wavelet transform (EWT-HT). Both methods can accurately identify the modal frequency, and the absolute difference between these two methods is equal to 0.003 Hz. The wind velocity results in a change of less than 1% in the modal frequency. The absolute difference between the modal damping ratios identified using SSI-COV and EWT-HT is significant and can reach 0.587%. The modal damping ratios are positively correlated with the mean wind velocities, which aligns with the quasi-steady assumption. In addition, the applicability of SSI-COV and EWT-HT is also evaluated using the standard deviation, coefficient of variation, and range dispersion indicators. The results show that the EWT-HT is more applicable to the identification of the modal parameters of long-span bridges under non-stationary wind velocities.

Keywords: Non-stationary wind velocity, Full-scale measurements, Modal identification, Empirical wavelet transform, Structural health monitoring, Theoretical aerodynamic damping

1 Introduction

The traditional stationary wind velocity model assumes that wind velocity in nature is stationary (Simiu and Yeo, 2019), and that the wind velocity signal can be decomposed into a deterministic constant mean value and a zero-mean stationary Gaussian stochastic process. However, according to the non-stationary model, the wind velocity should be decomposed into deterministic time-varying mean and zero-mean fluctuating

wind velocities. The critical step in applying the non-stationary model is extracting the time-varying mean wind velocity. Various methods have been developed to derive the slowly-varying trends of wind velocities, among which the empirical mode decomposition (EMD) and the discrete wavelet transform (DWT) are two popular and efficient approaches. Jiang et al. (2022) used the DWT to extract the time-varying mean wind velocity and selected the best wavelet decomposition level according to the turbulence energy. Cai et al. (2021) employed the EMD to extract the time-varying mean wind velocity and used quantitative methods to determine the optimal time-varying mean wind velocity. Tubino and Solari (2020) also discussed kernel regression techniques for extracting the time-varying mean wind velocity. In addition, the number of decomposed levels in the DWT-based or EMD-based approaches is usually determined empirically. Therefore, it is also a pressing issue to determine whether the remaining fluctuating wind velocity is stationary after subtracting the time-varying mean wind velocity from the original wind velocity.

The identification of the modal parameters of a bridge, including the modal frequencies, mode shapes and modal damping ratios, is an essential link in the state assessment of the bridge. In addition to the common modal frequencies and modal damping ratios, the changes in mode shape can in some cases reveal the damage position of the bridge. On the other hand, identifying the modal parameters under environmental excitation is complicated because the modal parameters of the bridge are strongly influenced by external environmental factors, such as temperature and wind velocity (Li et al., 2010). Of these factors, much work has been devoted to studying the effects of wind velocity on the modal parameters via long-term or short-term field measurements.

The measured bridge damping ratio varies with many factors, such as temperature, wind velocity, and dynamic displacement. When the displacement amplitude of the bridge deck is relatively small, i.e., less than 0.01 m, the wind velocity can be considered the main factor controlling the modal damping ratio, especially for the first three vertical modes (Wang et al., 2020). Through wind tunnel tests and field measurements, Chang et al. (2022) found that the aerodynamic damping ratio increases approximately linearly with the wind velocity. Hsu et al. (2020) showed that the modal parameters, especially the modal damping ratios, are significantly affected by the wind velocity. Meng et al. (2019) found that the modal frequencies of the first lateral and vertical modes depend on the wind velocity, and the modal frequency decreases with the increase of the wind velocity. Mao et al. (2017) pointed out that the damping ratio is more sensitive to the wind velocity than the modal frequency. Comanducci et al. (2015) found that the wind velocity changes significantly in the modal frequency. Many researchers have also concluded that environmental factors affect the modal parameters of the structure (Cross et al., 2013; Wang et al., 2016; Ubertini, 2013). However, the identification of the bridge modal parameters and the influence of the wind velocity on the bridge modal parameters both require further study.

This paper studies the identification of the bridge modal parameters under various wind velocities using field measurement data. Wind characteristics under stationary and non-stationary models are analyzed and compared in detail. The covariance-driven stochastic subspace system identification method (COV-SSI) and Hilbert transform methods based on the improved empirical wavelet transform (EWT-HT)

are then applied to identify the modal frequency and modal damping ratio of the two long-span bridges. The least squares fitting method is applied to obtain the relationships between the identified modal parameters and the wind velocities. The applicability of these two identification methods is also analyzed.

2 Data source

The Pingtan Straits Rail-cum-Road Bridge (PSRB) is located on China's southeast coast, to the northwest of the Taiwan Strait. With a total length of 16.34 km, the bridge is the world's longest cross-strait rail-cum-road bridge, and China's first cross-strait rail-cum-road bridge. The upper layer connects the Beijing-Taipei highway, one of the main longitudinal lines in China's national highway plan. The lower layer is the critical control project of the Fuzhou-Pingtan Railway, which is also an extension of the Hefei-Fuzhou high-speed railway. The Xihoumen Bridge (XB) is a cross-sea bridge in Zhoushan city, Zhejiang Province, China, above the Xihoumen cross-sea waterway. It is one of the components of the Yongzhou highway and an essential part of the Zhoushan Cross-Sea Bridge project. The main bridge is a two-span continuous semi-floating steel box girder suspension bridge with a main span of 1650 m, the fifth-longest in the world and the third-longest in China. The locations of the two investigated bridges and the observation points on the PSRB are shown in Fig. 1.

An ultrasonic anemometer and accelerometer are installed on the PSRB Guyumen cable-stayed bridge with a main span of 364 m (Yan et al., 2020). The sampling frequencies of the ultrasonic anemometer and accelerometer are 4 Hz and 51.2 Hz, respectively. During the observation period, the bridge was in the maximum single cantilever state (as shown in Fig. 1). In addition, the XB is taken as the comparison

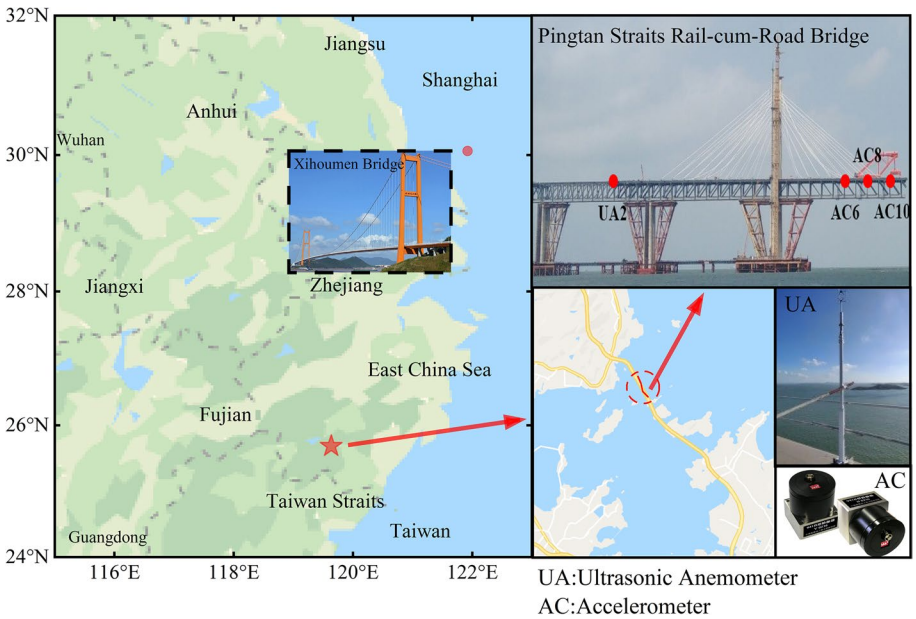

Fig. 1 Locations of two investigated bridges and observation points on PSRB

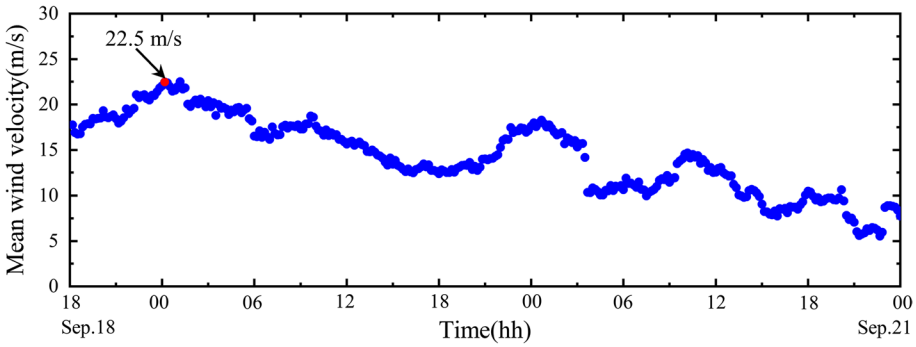

Fig. 2 Measured 10-min mean wind velocities during PSRB observation period

subject to verify the findings of this study, and it was already open to traffic when it was observed (Wang et al., 2018).

3 Wind characteristics

3.1 Stationary and non-stationary models

In the stationary model, the wind velocity is treated as a constant mean plus a zero-mean stationary random process, as follows:

$$U(t) = \overline{U}(t) + u(t) \tag{1}$$

where $U(t)$ is the wind velocity; $\overline{U}(t)$ is the constant mean over a time interval T, which is 10 min in this study; $u(t)$ is the fluctuating component.

In the non-stationary model, the wind velocity is decomposed into the deterministic time-varying mean and a zero-mean fluctuating component, as follows:

$$U(t) = \widetilde{U}^*(t) + u^*(t) \tag{2}$$

where $\widetilde{U}^*(t)$ is the deterministic time-varying mean wind velocity reflecting the wind velocity's temporal trend; $u^*(t)$ is the fluctuating wind velocity component that can be modeled as a zero-mean stationary process.

Figure 2 shows the measured 10-min mean wind velocity starting at 18:00 on September 18, 2019 (Beijing Time) and ending at 00:00 on September 21, 2019. During the first few hours of the wind records, the 10-min mean wind velocity increased continuously, reached its peak value of about 22.5 m/s at about 01:00–02:00 on September 19, and then gradually decreased to 5 m/s.

3.2 Time-varying mean wind velocity

Each recorded 10-min wind velocity is approximately non-stationary. Extracting the time-varying mean wind velocity is the first step under the non-stationary model. The DWT-based approach with the db10 wavelet is used to extract the time-varying mean wind velocity in this study. Another critical step is judging whether the extracted time-varying mean wind velocity is reasonable. In other words, after extracting the time-varying mean wind velocity, it is necessary to employ a rational stationarity test to check whether the remaining fluctuating wind velocity is stationary.

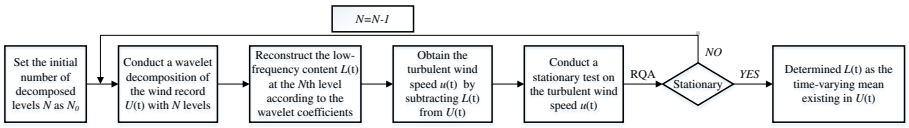

Fig. 3 General framework of self-adaptive approach to determining time-varying mean wind velocity

3.2.1 Stationarity test: recurrence plot and recursive quantitative analysis (RQA)

The physical meaning of the recurrence plot can be expressed as follows: let the track $\{X_i\}_{j=1}^{n}$ of the one-dimensional time series $\{x(t_i), i = 1, 2, \cdots, n\}$ in state space, and check whether the distance between point X_i and point X_j in space is less than the set threshold ε. When the distance between two points is less than or greater than the threshold ε, it indicates that these two points are recursive or non-recursive, as represented by black or white dots (Yang, 2011; Chen and Yang, 2012).

The macro characteristics of the recurrence plot can describe the overall features of the system. According to the different macro graphical characteristics of the recurrence plot, it can be divided into Homogeneous mode, Periodic mode, Drift mode and Disrupted mode. Different models have different graphical characteristics, which accurately reflect the internal change law of the system.

In order to quantitatively analyze the macro pattern in the recurrence plot, Webber and Zbilut (1994) proposed conducting a quantitative analysis of the recurrence plot, or, in other words, the distribution characteristics of the basic graph points and line segments in the statistical graph. This method is called recursive quantitative analysis. The recursive quantitative analysis indicators can be roughly divided into periodic, nonlinear and non-stationary types. This study mainly focuses on the non-stationarity index in the recursive quantitative analysis index, also called the lamellar degree (LAM). The LAM refers to the percentage of recursive points constituting the vertical line structure in the overall diagram. The calculation formula is:

$$LAM = \frac{\sum_{v=v_{min}}^{N} vP(v)}{\sum_{v=1}^{N} vP(v)} \tag{3}$$

where $P(v)$ is the sum of the number of vertical lines with length v, and the minimum vertical line length v_{min}, is usually 2. The size of the layered degree is usually inversely proportional to the number of independent recursive points in the recursive graph, which shows to some extent the relative velocity of the change of the system, and thus reflects the system's stability.

The smaller the values of the layered degree, the better the stability of the signal. On the other hand, the larger the values of the layered degree, the worse the stationarity of the signal.

3.2.2 Extracting time-varying mean wind velocity based on RQA

The self-adaptive DWT-based approach based on RQA was applied to extract a reasonable time-varying mean wind velocity. Figure 3 shows the general framework

of this approach. According to the presented scheme, a time-varying mean can be derived automatically according to the signal stationarity.

The following four main steps can describe the principle of this self-adaptive approach. By following this framework, the inherent time-varying mean in a wind record can be derived based on signal stationarity. Once the underlying trend is removed, the residual turbulent wind velocity will be stationary.

Step 1: Determine the maximum level that can be decomposed by DWT using Eq. 4, which is derived from the decomposition mechanism of the Mallat algorithm (Mallat, 1989). Then, set the initial number of decomposed levels N as N_0;

$$N_0 = log_2(T \cdot s) \tag{4}$$

where N_0 is the maximum decomposed level for DWT; T is the time interval; s is the sampling frequency of the wind record.

Step 2: Conduct a wavelet decomposition of the wind record U(t) with N levels. Then reconstruct the low-frequency content L(t) at the Nth level according to the wavelet coefficients. The turbulent wind velocity u(t) can thus be obtained by subtracting L(t) from U(t);

Step 3: Conduct a stationary test on the turbulent wind velocity u(t). In this study, RQA is employed. If the obtained u(t) can be treated as stationary based on the prescribed threshold, go directly to the final step. Otherwise, take N as $N-1$ and go to Step 2;

Step 4: Determine the time-varying mean existing in U(t) as L(t).

Figure 4 shows the time histories of three fluctuating wind velocity components of the maximum 10-min wind velocity (22.5 m/s, as shown in Fig. 2). The constant and time-varying mean wind velocities under the stationary and non-stationary models are also depicted in this figure. The constant and time-varying mean values in the three directions are different.

3.2.3 Comparison between stationary and non-stationary models

The turbulence intensity is a parameter describing the degree of the fluctuating wind velocity's variation with time and space. It is the ratio of the standard deviation of the fluctuating wind velocity to the mean wind velocity. The calculation formulas under the stationary and non-stationary models are as follows:

$$\text{Stationary model } I_a = \frac{\sigma_a}{\overline{U}}, (a = u, v, w) \tag{5}$$

$$\text{Non} - \text{stationary model } I_a^* = \frac{\sigma_a^*}{\overline{U}}, (a = u, v, w) \tag{6}$$

where a is the longitudinal, lateral and vertical fluctuating component; I_a and I_a^* are the turbulence intensity of the a fluctuating component under the stationary and non-stationary models, respectively; σ_a and σ_a^* are the standard deviations of the a fluctuating component under the stationary and non-stationary models, respectively.

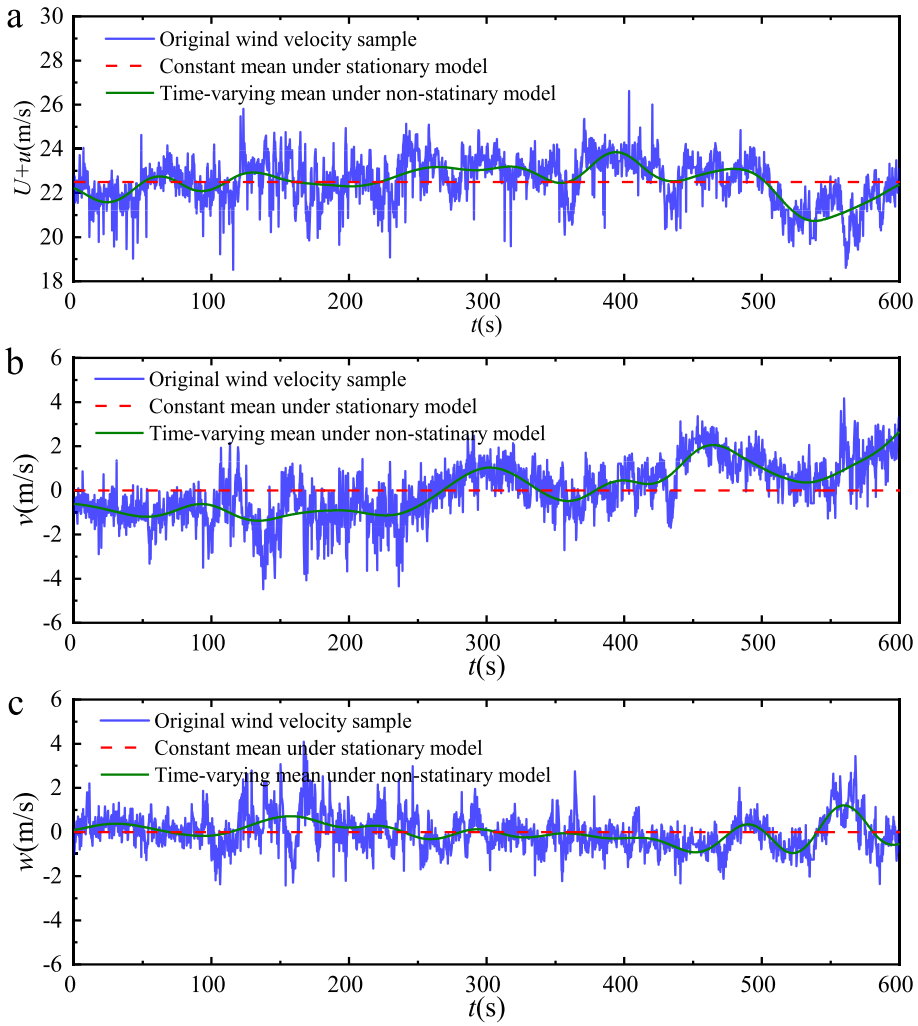

Fig. 4 Time histories of three fluctuating wind velocity components: **a** Longitudinal component; **b** Lateral component; **c** Vertical component

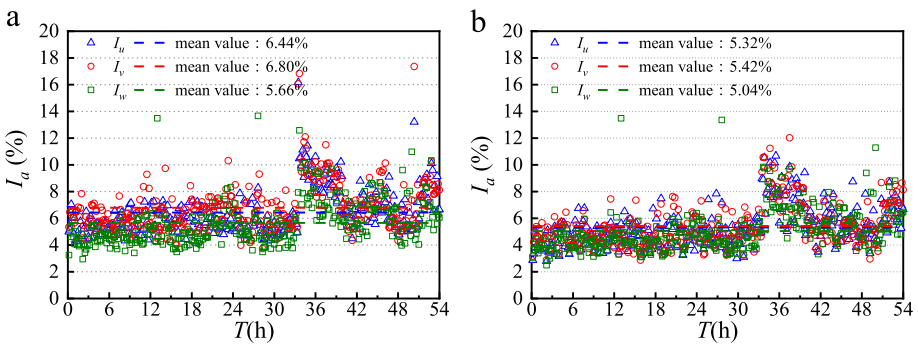

Fig. 5 Turbulence intensities during PSRB observation period: **a** Stationary model; **b** Non-stationary model

Figure 5 compares the turbulence intensities under the stationary and non-stationary models. The mean values of the longitudinal, lateral, and vertical turbulence intensity under the stationary model are respectively 6.44%, 6.80% and 5.66%, which are greater

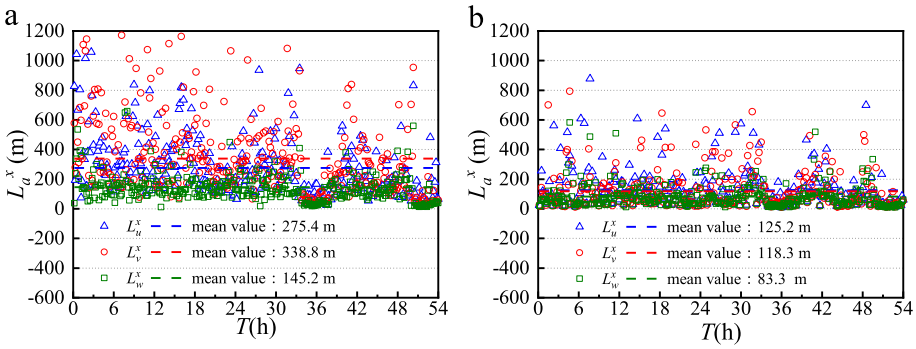

Fig. 6 Turbulence integral scales during PSRB observation period: **a** Stationary model; **b** Non-stationary model

than the mean turbulence intensity values (5.32%, 5.42% and 5.04%, respectively) under the non-stationary model. This difference is due to the reduction of the mean square deviation of the fluctuating wind velocity time history and turbulence intensity after excluding the time-varying mean wind velocity.

According to China's Wind-Resistant Design Specification for Highway Bridges (JTG/T 3360–01-2018), the recommended longitudinal turbulence intensity at a height of 70 m to 100 m under a class A landform is 11%. The mean values of the longitudinal turbulence intensity under the stationary and non-stationary models are significantly lower than the recommended value.

The turbulence integral scale is used to characterize the wind field's mean scale of the vortices. Based on the Taylor hypothesis, the autocorrelation function integral method is usually used for calculation. The formulas under the stationary and non-stationary models are as follows:

$$\text{Stationary model } L_a^x = \frac{\overline{U}}{\sigma_a^2} \bullet \int_0^\infty R(\tau)d\tau, (a = u, v, w) \tag{7}$$

$$\text{Non} - \text{stationary model } L_a^{x*} = \frac{\widetilde{U}}{\sigma_a^{2*}} \bullet \int_0^\infty R(\tau)d\tau, (a = u, v, w) \tag{8}$$

where L_a^x and L_a^{x*} are the turbulence integral scales of the a fluctuating component in the longitudinal x direction under the stationary and non-stationary models, respectively; $R(\tau)$ is the autocovariance function of the a fluctuating component; σ_a^2 and $\sigma_a^{2^*}$ are the variances of the a fluctuating component under the stationary and non-stationary models, respectively.

Figure 6 compares the turbulence integral scales under the stationary and non-stationary models. The mean values of the longitudinal, lateral and vertical turbulence integral scales under the stationary model are respectively 275.4 m, 338.8 m and 145.2 m, which are greater than the corresponding values (125.2 m, 118.3 m and 83.3 m, respectively) under the non-stationary model.

The mean turbulence integral scale of the longitudinal fluctuating component under the stationary model (275.4 m) is larger than the recommended value of 140 m (JTG/T 3360–01-2018). The calculated value under the non-stationary model (125.2 m) is closer to the recommended value.

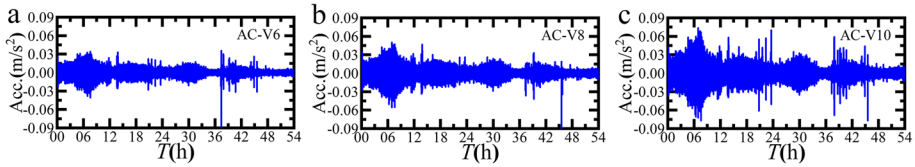

Fig. 7 Acceleration responses at three PSRB observation points: **a** AC-V6; **b** AC-V8; **c** AC-V10

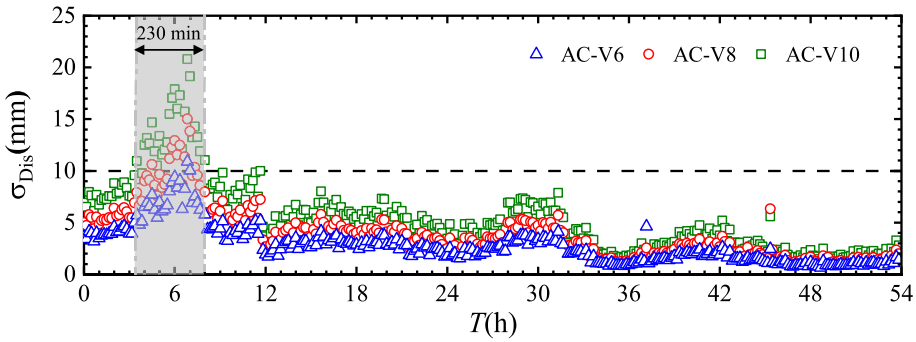

Fig. 8 Displacement responses at three PSRB observation points

4 Modal parameter identification

4.1 Acceleration responses

Vertical acceleration responses at three observation points (as shown in Fig. 1) from 18:00 on September 18 to 24:00 on September 20, 2019 (as shown in Fig. 2) were selected as input signals for modal parameter analysis. Figure 7 shows the acceleration responses after the low-pass filtering process with a cut-off frequency of 4 Hz. The closer the measurement point to the cantilever end, the greater the vertical acceleration during the observation period. The vertical acceleration of the AC10 measurement point is significantly greater than that of the other two observation points, and it was selected to be input data for the next modal parameter analysis.

The displacement responses can be obtained by the frequency domain integration of the structural acceleration responses. Figure 8 gives the corresponding vertical displacement responses at a time interval of 10 min. The vertical displacement response of measurement point AC10 is the largest, AC8 is the second largest and AC6 is the smallest, which is consistent with the acceleration response results. The time during which the displacement exceeded 0.01 m for the whole observation period was only 7% of the total time, so the variation of the damping ratio in this case study can be considered to be unrelated to the displacement amplitude (Wang et al., 2020).

4.2 SSI-COV and EWT-HT identification methods

The SSI-COV is a traditional modal parameter identification method that is widely used in civil engineering (Van Overschee and De Moor, 1997; Zou et al., 2020). Figure 9 shows the process of identifying the modal parameters using the SSI-COV method.

In recent years, time–frequency signal processing techniques such as the empirical wavelet transform (EWT) have been widely used for the modal parameter estimation of civil structures. The EWT (Gilles, 2013) adaptively divides the Fourier spectrum of

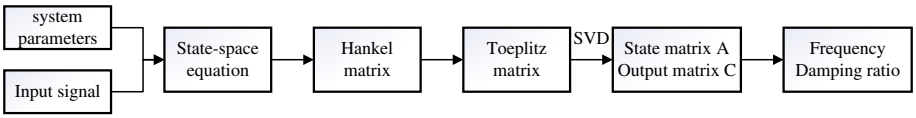

Fig. 9 SSI-COV modal parameter identification framework

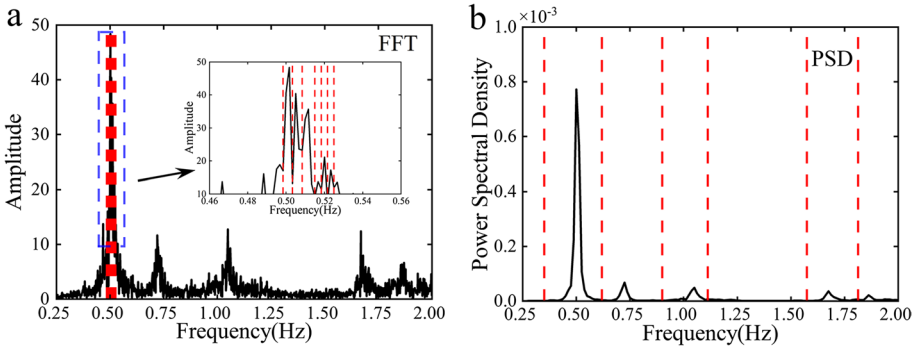

Fig. 10 Comparison results between two bases for dividing frequency band boundary: **a** Fourier spectrum; **b** Power spectral density

the analyzed multi-component signal. It constructs a group of wavelet filter banks to filter the divided spectrum and decompose the multi-component signal into a series of amplitude modulation and frequency modulation single-component components with a tightly-supported Fourier spectrum.

In order to improve the boundary estimation of Gilles' method when dealing with low signal-to-noise ratio multi-component signals, the power spectral density spectrum was employed to divide the signal frequency bands in this study, rather than the Fourier spectrum. Figure 10 compares the results using the Fourier spectrum as the basis of the frequency band division with those using the power spectral density. The power spectral density spectrum is smoother than the Fourier spectrum. Even in noisy cases, it can still identify each mode order frequency. The power spectral density curve of every significant spectral peak can be the signal of a single modal, and the band boundary can be more accurately estimated to establish the corresponding wavelet filter bank and better separation signals for each order mode.

For the selection of the frequency band boundary, Gilles (2013) proposed the method of selecting the mean value of two adjacent peaks of the spectrum as the boundary, which is very effective for signals with no noise and simple signal components. However, for noisy signals, signal decomposition based on Gilles' method is unsuitable due to the existence of small peak values caused by noise in the signal's spectrum. In order to reduce the influence of noise on signal decomposition, Amezquita-Sanchez et al. (2017) proposed an improved frequency band selection method that uses two minima adjacent to the maximum peak of the spectrum as the boundary. The improved method can better isolate the main vibration frequency and noise, and reduce the influence of the noise to the greatest extent.

Through the EWT, the original signal sequence was decomposed into the modal response component of the structure, which was composed of the free vibration

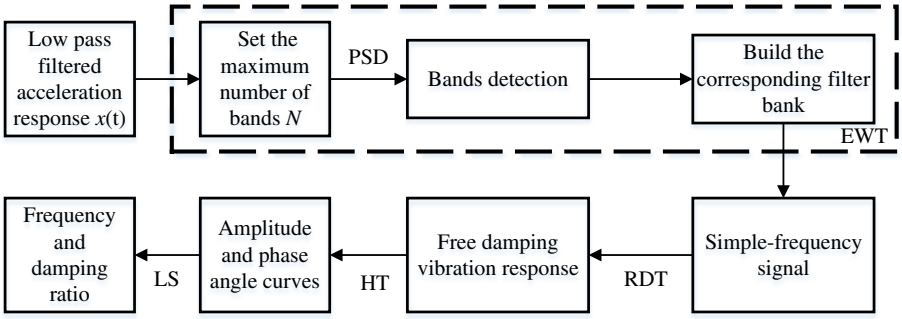

Fig. 11 EWT-HT modal parameter identification framework

response and the forced vibration response. The free attenuation response was obtained by the random decrement technique (Ibrahim, 2001) for the single component. Its free attenuation response can be expressed as:

$$v(t) = A_0 e^{-\zeta\omega_0 t} cos(\omega_d t + \phi_0) \tag{9}$$

where ω_0 is the circular frequency; ω_d is the damping frequency; ζ is the damping ratio and A_0 is a constant. The analytic signal $z(t)$ corresponding to $v(t)$ is:

$$z(t) = v(t) + i\widetilde{v}(t) = A(t)e^{-i\theta(t)} \tag{10}$$

where $\widetilde{v}(t)$ is the Hilbert transform of $v(t)$. For general engineering structures, the amplitude $A(t)$ and phase $\theta(t)$ in the formula can be further expressed as:

$$A(t) = A_0 e^{-\zeta\omega_0 t} \tag{11}$$

$$\theta(t) = \omega_d t + \phi_0 \tag{12}$$

By using logarithms and differential operators, the amplitude function and phase function of Eq. 11 and Eq. 12 are respectively transformed to obtain:

$$lnA(t) = -\zeta\omega_0 t + lnA_0 \tag{13}$$

$$\omega_d = \frac{d\theta(t)}{dt} \tag{14}$$

Obviously, the damping frequency ω_d can be obtained from the slope of the phase function $\theta(t)$ corresponding to the equation of the line in Eq. 14. When the slope $\zeta\omega_0$ of Eq. 13 of the line is determined, the ω_0 and the damping ratio ζ can be obtained by the following equation:

$$\omega_d = \omega_0\sqrt{1-\zeta^2} \tag{15}$$

Figure 11 shows the modal parameter identification calculation process of EWT-HT. The first step of this method is setting the maximum number of bands and calculating the power spectral density spectrum of the low-pass filtered acceleration response to determine the boundaries. Then, according to the divided frequency

bands, the corresponding filter banks are built and multiple simple-frequency signals are obtained. The simple-frequency signals are treated by the random decrement technique to obtain the free damping vibration response, and the response amplitude and phase angle curves are found using the Hilbert transform. Finally, the least squares fitting method is used to extract the modal parameters.

4.3 Identification results and analysis

Based on the quasi-steady assumption, the aerodynamic force of the bridge deck can be expressed by the derivation of the static three-component coefficient and its first derivatives as follows (Kareem and Gurley, 1996; Kim et al., 2019). The theoretical aerodynamic damping ratio of the vertical bending motion is derived when the torsional motion is ignored:

$$\zeta_{\text{aero}} = \frac{\rho B U}{8\pi f_i m}\left(\left[C_L^{'}\right]_{\alpha=0} + C_D\right) \tag{16}$$

where ρ is the air density, equal to 1.225 kg/m^3; B is the width of the bridge deck, which is 36.8 m; m is the mass per unit length, which is 34286 kg/m; f_i is the natural frequency of the structure of i mode order (Hz); C_L is the lift coefficient; α is the wind attack angle; $C_L^{'}$ is the first derivative of the lift coefficient with respect to radians, which is 4.3154; C_D is the drag coefficient, which is 0.2314 (Zhang, 2019).

According to Eq. 16, when the bridge structure is entirely determined, the aerodynamic damping ratio of the bridge deck is positively correlated with the mean wind velocity. This paper uses two methods, including the mentioned COV-SSI and EWT-HT, to identify the first three vertical bending modal parameters of the PSRB. The relationships between the mean wind velocity and modal parameters are linearly fitted by Eq. 17 and Eq. 18:

$$f_i = a_1 \times U + b_1 \tag{17}$$

$$\zeta_i = a_2 \times U + b_2 \tag{18}$$

where U is the 10-min mean wind velocity in this study (m/s); f_i is the modal frequency of the bridge (Hz); ζ_i is the modal damping ratio of the bridge; a_1, a_2, b_1 and b_2 are floating parameters that must be fitted using measured data.

In addition, the standard deviation (σ), coefficient of variation (c_v) and range (R) are used to judge the dispersion of the identified modal parameters using the two methods, as follows:

$$\sigma = \sqrt{\frac{\sum_{i=1}^{n}\left(X_i - \overline{X}\right)^2}{n-1}} \tag{19}$$

$$c_v = \frac{\sigma}{\overline{X}} \tag{20}$$

$$R = X_{max} - \mathrm{X}_{min} \tag{21}$$

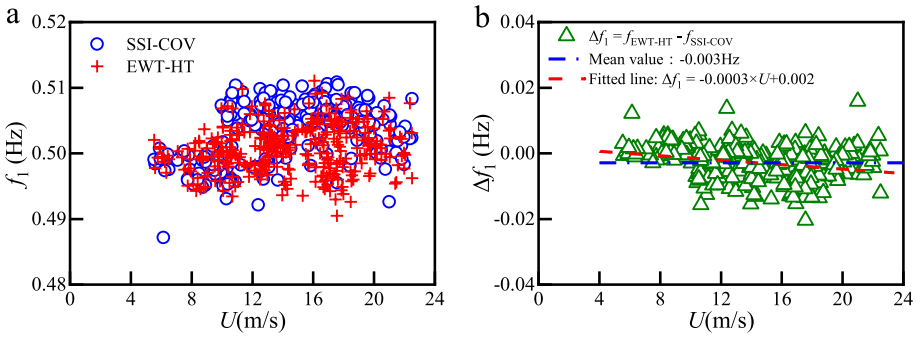

Fig. 12 Measured modal frequencies of first-order vertical bending of PSRB: **a** Two identification methods; **b** Difference between two identification methods

where X is the modal frequency or modal damping ratio; $\overline{X}$ is the mean value of X; X_{max} is the maximum value of X; X_{min} is the minimum value of X; i is the sample number; n is the total number of samples.

4.4 Modal frequency

Figure 12 shows the measured modal frequencies of the first-order vertical bending of the PSRB under various mean wind velocities using the SSI-COV and EWT-HT identification methods. The two identification methods can accurately identify the first-order vertical bending modal frequencies, but the SSI-COV identification method results in a few extreme values. The mean value of the difference between the two identification methods is very small and equal to -0.003 Hz. The difference decreases with the increase of the mean wind velocity. The greater the mean wind velocity, the more significant the difference between the two methods. The modal frequency identified using SSI-COV is quite large and has a few extreme values. This may be because there are many false modes in the application of the SSI-COV method. These false modes mainly arise from the system parameters and the input signal. The system parameters are also known as the system order, and this order, which must be empirically pre-determined, results in the generation of false modes. In addition, the input signal does not satisfy the white noise assumption, and the environmental influence on the output signal can also result in the generation of false modes.

Before the correlation analysis, the sample sizes of different wind velocity intervals were statistically analyzed. Figure 13 shows that the sample sizes are different in different wind velocity ranges. The samples are not evenly distributed across each entire wind velocity range, and the sample size in the wind velocity range of 8–20 m/s accounts for 85% of the total sample size. Since this study seeks the linear relationship between the modal parameters and the mean wind velocity, the linear fitting results using all the sample data cannot truly reflect the linear relationship between the sample data under such a distribution. Therefore, the median of the sample data within each wind velocity interval is set as 1 m/s for fitting, which can reflect the overall level and remove the influence of any extreme values.

Figure 14 shows the relationship between the measured modal frequency and wind velocity in the first three vertical bendings of the PSRB using the SSI-COV and EWT-HT identification methods. The first three vertical bending frequency results

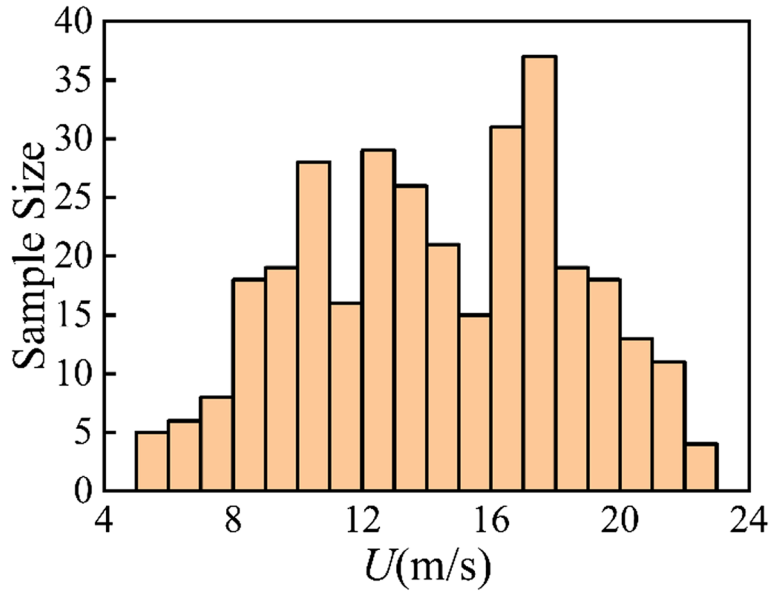

Fig. 13 Sample sizes in different wind velocity ranges (1 m/s)

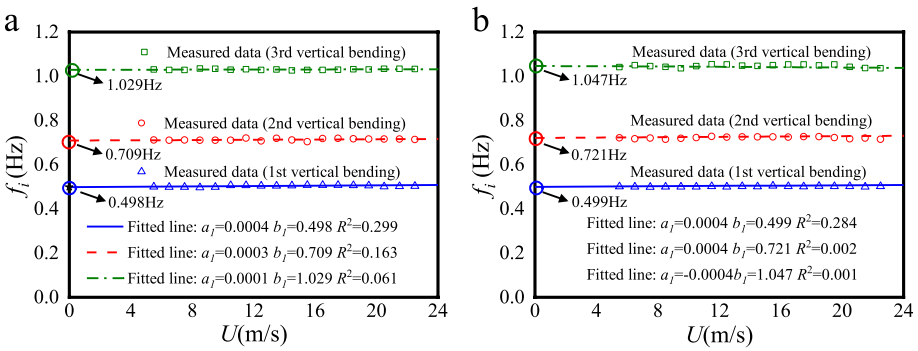

Fig. 14 Relationship between measured modal frequency and wind velocity in first three vertical bendings of PSRB: **a** SSI-COV; **b** EWT-HT

using the two methods are basically identical, and the fitting results show that the variation of the modal frequency with the mean wind velocity is relatively small. There is almost no correlation between the modal frequency and the mean wind velocity. When the mean wind velocity is zero, the structural frequency (the intercept of the fitting line) of the first-order vertical bending to the third-order vertical bending indicates that the identification results of the two identification methods are effective and accurate.

4.5 Modal damping ratio

Figure 15 shows the measured modal damping ratios of the first-order vertical bending of the PSRB under various mean wind velocities using the SSI-COV and EWT-HT identification methods. The mean value of the difference between the two identification methods is very small and equal to -0.587%, and the difference decreases with the increase of the mean wind velocity. Similarly, the SSI-COV method results in some

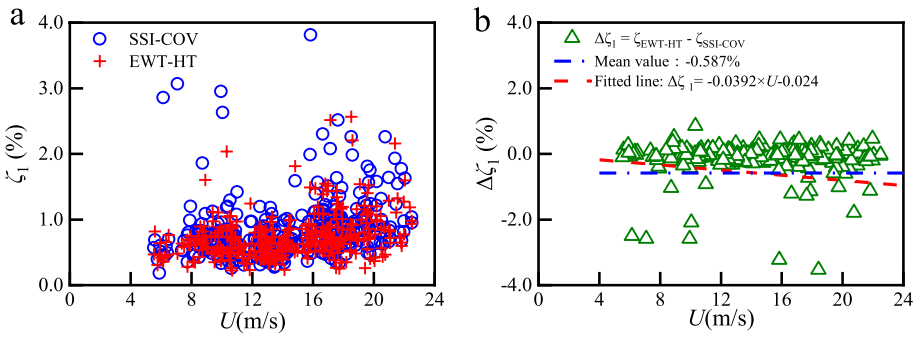

Fig. 15 Measured modal damping ratio of first-order vertical bending of PSRB: **a** Two identification methods; **b** Difference between two identification methods

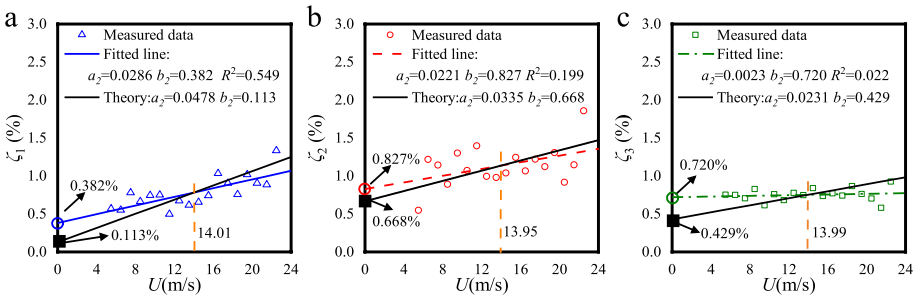

Fig. 16 Relationship between measured modal damping ratios and wind velocity in the first three vertical bendings of PSRB using SSI-COV: **a** First-order; **b** Second-order; **c** Third-order

extreme damping ratios and the identified damping ratios are more extensive than those identified using the EWT-HT method. Because the modal frequency and modal damping ratio of each sample always appear in pairs, the sample number distribution of the damping ratio in different wind velocity ranges is the same as that in Fig. 13. The identified modal damping ratios need to be processed using the same approach before the linear fitting.

Figures 16 and 17 show the relationship between the identified modal damping ratio and the mean wind velocity using the SSI-COV and EWT-HT methods, respectively. According to the fitted curves and R^2 results, the first-order vertical bending damping ratio has the strongest correlation with the mean wind velocity, and it increases with the increase of the mean wind velocity. The correlation between the second-order vertical bending damping ratio and the mean wind velocity is weaker than that of the first-order vertical bending, while the third-order vertical bending damping ratio can be regarded as having no correlation with the mean wind velocity. Figure 16 shows that when the mean wind velocity is zero, the intercept of the fitting curve of the damping ratio of the first three vertical bendings using the SSI-COV method (namely, the structural damping ratios), are 0.382%, 0.827% and 0.720%, respectively, which are larger than the structural damping ratio obtained by the theoretical aerodynamic damping ratio curve of the first three vertical bendings, i.e., 0.113%. 0.668% and 0.429%. Both the structural damping ratios obtained by the measured damping fitting curve and the structural damping ratio obtained by the theoretical aerodynamic

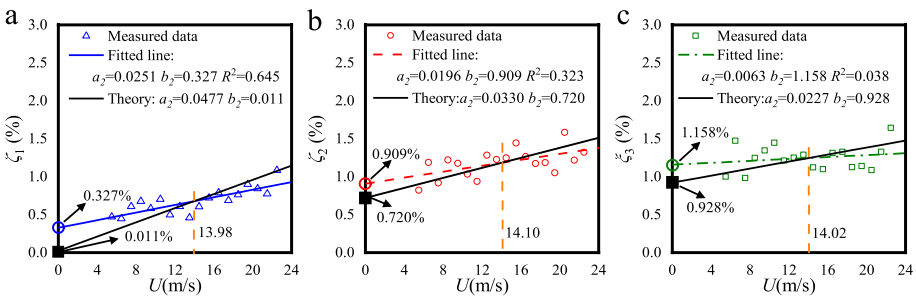

Fig. 17 Relationship between measured modal damping ratios and wind velocity in first three vertical bendings of PSRB using EWT-HT: **a** First-order; **b** Second-order; **c** Third-order

damping ratio curve are different from the structural damping ratio of 0.5% recommended by the Chinese structural specification (JTG/T 3360–01-2018). Similarly, Fig. 17 shows that the structural damping obtained from the fitted curve of the damping ratios identified by the EWT-HT method is greater than that obtained from the theoretical aerodynamic damping curve. At the same time, regardless of the structural damping ratios obtained from the fitting curve of the measured damping ratios, or the structural damping ratios obtained from the curve of the theoretical aerodynamic damping ratios, there is no phenomenon through which the structural damping ratio decreases with the increase of the mode order, which is similar to the results in Li et al. (2011). Comparing the two identification methods, the fitting results of the damping ratios identified using the EWT-HT method are better than those found with the SSI-COV method in terms of R^2 values. For the comparison fitted curve and theoretical curve, no matter which identification method is applied or which mode order is identified, the intersection point of the two curves is near the mean wind velocity of approximately 14 m/s. When the mean wind velocity is less than 14 m/s, the value of the fitted curve is greater than that of the theoretical curve. On the contrary, when the mean wind velocity is greater than 14 m/s, the theoretical curve value is greater than the fitted curve value.

Figure 18 shows the differences between the identified damping ratios of the first three vertical bendings using two methods. The mean differences between the identified damping ratios are -0.104%, 0.045% and 0.494%, respectively. The standard deviations of the identified damping ratios are 0.007%, 0.088% and 0.031%, respectively. To sum up, the difference between the two methods in identifying the first-order vertical bending damping ratio is small, while the differences in the identification of the damping ratios of the second-order and third-order vertical bendings are large.

The Pearson correlation coefficient is used to quantify the similarity between the modal damping ratios identified by different methods. The correlation coefficient r is defined as:

$$r(Y_1, Y_2) = \frac{Cov(Y_1, Y_2)}{\sqrt{Var[Y_1]Var[Y_2]}} \tag{22}$$

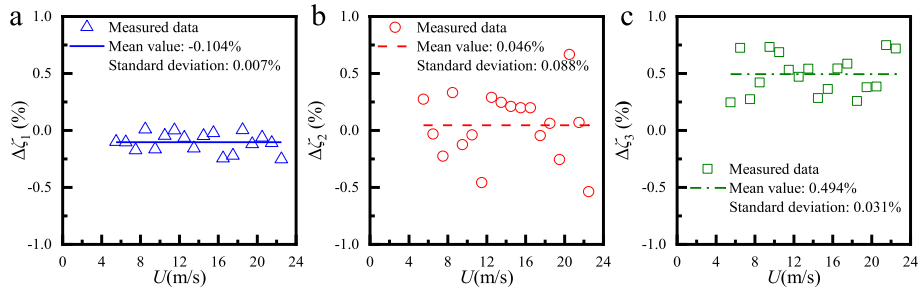

Fig. 18 Difference between identified damping ratios of first three vertical bendings using SSI-COV and EWT-HT: **a** First-order; **b** Second-order; **c** Third-order

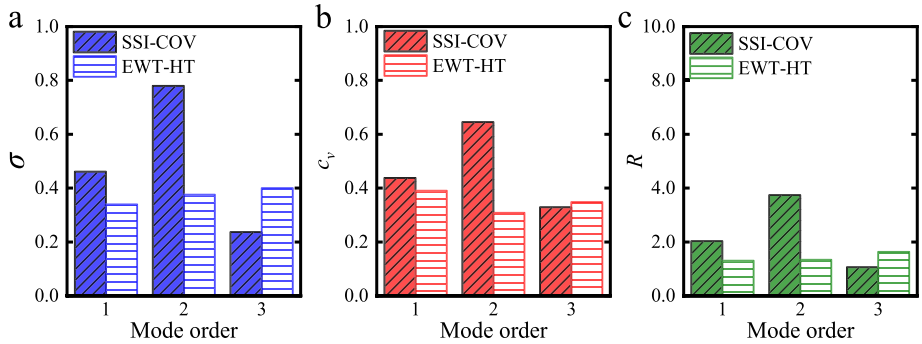

Fig. 19 Dispersion index of different methods at 20 m/s wind velocity: **a** Standard deviation σ; **b** Coefficient of variation c_v; **c** Range R

where Y_1 is the modal damping ratio identified by the SSI-COV method; Y_2 is the modal damping ratio identified by the EWT-HT method; $Cov(Y_1, Y_2)$ is the covariance of Y_1 and Y_2; $Var[Y_1]$ is the variance of Y_1; $Var[Y_2]$ is the variance of Y_2.

The correlation coefficients of the damping ratios of the first three vertical bendings identified by the different methods are 0.92, 0.16 and 0.17, respectively. The first-order vertical damping ratios identified by these two methods are highly consistent. In contrast, the similarities between the second-order and third-order damping ratios identified using the two methods are unsatisfactory.

In this study, the discreteness of the identification results of the two methods is analyzed to compare the methods' engineering applicability and practicability. A mean wind velocity of 20 m/s is selected (for example, the mean wind velocity of 19–21 m/s is selected at 20 m/s) to calculate the standard deviation (σ), coefficient of variation (c_v) and range (R), as well as to draw a bar chart to analyze the dispersion of the results calculated by the different methods. Figure 19 shows that for the first- and second-order vertical bending modes, the three parameters related to discreteness using the SSI-COV method are all larger than those using the EWT-HT method, especially for the second-order vertical bending mode. However, it is just the opposite for the third-order mode. This is consistent with the results presented in Figs. 16 and 17. The identification results of the SSI-COV method appear to be more discrete. The EWT-HT method has better control over the calculation discreteness.

Table 1 Statistics of fitting parameters of identified modal frequencies of PSRB and XB

Bridge	Mode order	Identification method					
		SSI-COV			EWT-HT		
		a_1	b_1	R^2	a_1	b_1	R^2
PSRB	1	0.00040	0.498	0.299	0.00040	0.499	0.284
	2	0.00030	0.709	0.163	0.00040	0.721	0.002
	3	0.00010	1.029	0.061	-0.00040	1.047	0.001
XB	1	0.00004	0.095	0.160	0.00001	0.095	0.198
	2	-0.00004	0.130	0.144	-0.00002	0.132	0.138
	3	-0.00002	0.229	0.088	0.00000	0.230	0.048

Table 2 Statistics of fitting parameters of identified modal damping ratios of PSRB and XB

Bridge	Mode order	Identification method						Recommended structural damping (%)
		SSI-COV			EWT-HT			
		a_2	b_2	R^2	a_2	b_2	R^2	
PSRB	1	0.0286	0.382	0.549	0.0251	0.327	0.645	0.500
	2	0.0221	0.857	0.199	0.0196	0.909	0.323	0.500
	3	0.0023	0.720	0.022	0.0063	1.158	0.063	0.500
XB	1	0.0326	0.667	0.398	0.0561	0.759	0.563	0.500
	2	0.0052	0.709	0.080	0.0369	0.251	0.771	0.500
	3	0.0077	0.195	0.249	0.0309	0.076	0.755	0.500

5 Discussion

In Section 4, the modal parameter identification results of the PSRB are obtained. In order to reach a more effective and accurate conclusion, the measured data of the XB are also analyzed and compared. Table 1 shows the fitting parameters of the identified modal frequencies of the PSRB and XB. The R^2 values of the first-order linear fitting between the modal frequency and the mean wind velocity of the two bridges are all less than 0.30, indicating that there is no first-order linear relationship between the modal frequency and the mean wind velocity, or that the first-order linear relationship is weak. At the same time, the absolute slope value $|a_1|$ of the linear fitting curve of the PSRB modal frequency identification results is less than 0.0004. In the entire wind velocity range, the variation of the modal frequency caused by the increase of the wind velocity is $0.0004 \times 22.5 = 0.009$Hz, accounting for about 1.7% of the first-order structure frequency. Similarly, the absolute slope value of the primary linear fitting curve of the XB modal frequency identification results is less than 0.00004, and the variation of the modal frequency with the mean wind velocity is $0.00004 \times 21.6 = 0.00086$Hz, accounting for about 1% of the first-order structure frequency. The fluctuation of the second- and third-order modal frequencies with the wind velocity accounts for less than 1% of the corresponding structure frequency. Therefore, the mean wind velocity can be considered to have almost no effect on the modal frequency.

Table 2 shows the fitting parameters of the identified modal damping ratios of the PSRB and XB. The fitting parameter a_2 of the linear fitting curve of the modal damping ratios and the mean wind velocity of the two bridges is similar to the change rate of

Table 3 Statistics of dispersion indexes of identified modal damping ratios of PSRB and XB

Bridge	Mode order	Identification method					
		SSI-COV			EWT-HT		
		σ	c_v	R	σ	c_v	R
PSRB	1	0.400	0.466	1.947	0.264	0.353	1.155
	2	0.897	0.676	4.297	0.511	0.373	2.018
	3	0.305	0.384	1.380	0.405	0.329	1.730
XB	1	0.671	0.579	3.064	0.656	0.450	2.629
	2	0.620	0.694	2.720	0.373	0.515	1.418
	3	0.173	0.548	0.641	0.278	0.595	1.154

the theoretical aerodynamic damping, which is positive. Furthermore, the linear fitting curve of the modal damping ratios and the mean wind velocity shows a positive correlation trend. However, the fitting parameter a_2 of the fitted curve is lower than the change rate of the theoretical aerodynamic damping, which may be due to the fact that in the actual environment, the modal damping ratios are not only affected by the mean wind velocity, but also the temperature, traffic flow and environmental noise. These factors constitute a complex non-stationary environment. The theoretical value only considers the influence of the mean wind of the steady incoming flow in an ideal environment. For this reason, some R^2 values are too small, especially those identified by the SSI-COV method. Compared with the SSI-COV method, the EWT-HT method has better recognition performance under non-stationary environmental excitation.

At the same time, when the mean wind velocity is 0, the fitting parameter b_2 of the fitting curve is the structural damping of the actual bridge, which cannot meet the requirements of the design specifications. For the PSRB, the actual structural damping of the first mode is lower than that recommended by the design code, while the actual structural damping of the second and third modes is more significant than that recommended by the design code. However, the result of the XB is the opposite of that of the PSRB. The actual structural damping of the first-order mode is greater than the recommended modal damping ratio (JTG/T 3360–01-2018), and the actual structural dampings of the second- and third-order modes are greater than the recommended value, except for the results identified by the SSI-COV method for the second-order mode. This phenomenon may be related to the type and state of the bridges.

Table 3 shows the dispersion indexes of the identified modal damping ratios of the PSRB and XB. The dispersion indexes are averaged in each meter wind velocity interval. Obviously, the three dispersion indexes of the modal damping ratios identified by the EWT-HT method are all smaller than those obtained by the SSI-COV method, except for the third-order result. However, for practical engineering, more attention is paid to the frequency and damping ratios of the lower mode orders, which occupy more energy. It is proven that the EWT-HT method can identify the modal parameters stably and effectively in practical engineering applications. Compared with the SSI-COV method, the EWT-HT method can better adapt to the complex non-stationary environments of actual situations and is more applicable to the identification of low-order modes.

6 Conclusions

The calculated turbulence intensity and turbulence integral scale under the non-stationary model are smaller than those under the stationary model, especially the turbulence integral scale. It is necessary to extract the time-varying mean of the wind velocity.

Both the SSI-COV and EWT-HT methods can accurately identify the modal frequencies of the PSRB. The absolute difference between these two methods is small, being equal to 0.003 Hz. The correlation between the modal frequency of the long-span bridge and the mean wind velocity is weak, and the wind velocity results in a change of less than 1% in the modal frequency.

The absolute difference between the identified modal damping ratio of the PSRB using the SSI-COV and EWT-HT methods is large and can reach up to 0.587%. The modal damping ratios are positively correlated with the mean wind velocities, especially the first- and second-order vertical bending modes, which is consistent with the curve trend of the theoretical aerodynamic damping ratios.

The identified structural damping ratios of the first three vertical bendings of the PSRB and XB differ from the structural damping ratio recommended by the Chinese structural specification, i.e., 0.5%.

The applicability of the SSI-COV and EWT-HT methods to thePSRB and XB is evaluated using dispersion indicators of standard deviation, coefficient of variation, and range. The EWT-HT method is more suitable for identifying the modal parameters of long-span bridges under non-stationary wind velocities and practical engineering.

Acknowledgements
The authors would like to thank Dr. Lei Ren at Xi'an Jiaotong University for his contribution to the preliminary data collection.

Authors' contributions
Formal analysis, S.L. and L.Y.; Funding acquisition, L.Y. and X.H.; Investigation, S.L. and L.Y.; Project administration, X.H.; Supervision, X.H. and H.G.; Writing—original draft, S.L.; Writing—review & editing, S.L. and L.Y. All authors have read and agreed to the published version of the manuscript.

Funding
The work described in this paper was supported by the National Natural Science Foundation of China (Grant 52178516, 51925808), and the Innovation-Driven Project of Central South University (No. 2020CX009). Any opinions and concluding remarks presented in this paper are entirely those of the authors.

Availability of data and materials
The datasets used and analyzed during the current study are available from the corresponding author on reasonable request.

Declarations

Competing interests
Xuhei He is an editorial board member for Advances in Bridge Engineering and was not involved in the editorial review, or the decision to publish, this article. All authors declare that there are no competing interests.

Received: 28 September 2022 Accepted: 1 November 2022
Published online: 16 December 2022

References

Amezquita-Sanchez JP, Park HS, Hojjat A (2017) A novel methodology for modal parameters identification of large smart structures using MUSIC, empirical wavelet transform, and Hilbert transform. Eng Struct 147:148–159
Cai K, Li X, Zhi LH, Han XL (2021) Extraction of optimal time-varying mean of non-stationary wind speeds based on empirical mode decomposition. Struct Eng Mech 77(3):355–368
Chang Y, Zhao L, Zou Y, Ge YJ (2022) A revised Scruton number on rain-wind-induced vibration of stay cables. J Wind Eng Ind Aerodyn 230:105166

Chen Y, Yang H (2012) Multiscale recurrence analysis of long-term nonlinear and non-stationary time series. Chaos, Solitons Fractals 45(7):978–987
Comanducci G, Ubertini F, Materazzi AL (2015) Structural health monitoring of suspension bridges with features affected by changing wind speed. J Wind Eng Ind Aerodn 141:12–26
Cross EJ, Koo KY, Brownjohn JMW, Worden K (2013) Long-term monitoring and data analysis of the Tamar Bridge. MSSP 35(1):16–34
Gilles J (2013) Empirical wavelet transform. IEEE Trans Signal Process 61(16):3999–4010
Hsu TY, Chien CC, Shiao SY, Chen CC (2020) Analysis of environmental and typhoon effects on modal frequencies of a power transmission tower. Sensors 20(18):5169
Ibrahim SR (2001) Efficient random decrement computation for identification of ambient responses. Proceedings of the 19th International Modal Analysis Conference (IMAC), Florida
Jiang F, Zhang M, Li Y, Yan T, Zhang J (2022) Field measurement analysis of wind parameters and non-stationary characteristics in mountainous terrain: focusing on cooling windstorms. J Wind Eng Ind Aerodyn 230:105175
Kareem A, Gurley K (1996) Damping in structures: Its evaluation and treatment of uncertainty. J Wind Eng Ind Aerodn 59:131–157
Kim S, Jung H, Kong MJ, Lee DK, An YK (2019) (2019) In-situ data-driven buffeting response analysis of a cable-stayed bridge. Sensors 19:3048
Li H, Li SL, Ou JP, Li HW (2010) Modal identification of bridges under varying environmental conditions: temperature and wind effects. Struct Control Health Moni 17(5):495–512
Li H, Laima SJ, Ou JP, Zhou WS, Yu Y, Li N, Liu ZQ (2011) Investigation of vortex-induced vibration of a suspension bridge with two separated steel box girders based on field measurements. Eng Struct 33(6):1894–1907
Mallat S (1989) Multiresolution approximations and wavelet orthonormal bases of L2(R). Trans Am Math Soc 315(1):69–88
Mao JX, Wang H, Xun ZX, Zou ZQ (2017) Variability analysis on modal parameters of Runyang Bridge during Typhoon Masta. Smart Struct Syst 19(6):653–663
Meng X, Nguyen DT, Owen JS, Xie Y, Psimoulis P, Ye G (2019) Application of GeoSHM system in monitoring extreme wind events at the Forth Road Bridge. Remote Sensing 11(23):2799
Ministry of Transportation and Communication of PRC (2018) JTG/T 3360–01–2018 Wind-Resistant Design Specification for Highway Bridges. China Communications Press Co., Ltd., Beijing
Simiu E, Yeo DH (2019) Wind Effects on Structures: Modern Structural Design for Winds, 4th edn. John Wiley & Sons, Inc, New York
Tubino F, Solari G (2020) Time varying mean extraction for stationary and non-stationary winds. J Wind Eng Ind Aerodyn 117:104187
Ubertini F (2013) On damage detection by continuous dynamic monitoring in wind-excited suspension bridges. Mecc 48(5):1031–1051
Van Overschee P, De Moor B (1997) Subspace Identification for Linear Systems: Theory-Implementation-Applications. Springer Science & Business Media, Berlin
Wang H, Mao JX, Huang JH, Li AQ (2016) Modal identification of Sutong cable-sstayed bridge during Typhoon Haikui using Wavelet transform method. J Perform Constr Facil 30(5):04016001
Wang SQ, Zhao L, Cao SY, Zhang YF, Yin F, Ge YJ (2018) (2018) A comparison study on gust factor considering non-stationary effects under typhoon and monsoon conditions. Adv Struct Eng 21(12):1853–1864
Wang H, Mao JX, Xu ZD (2020) Investigation of dynamic properties of a long-span cable-stayed bridge during typhoon events based on structural health monitoring. J Wind Eng Ind Aerodn 201:104172
Webber CL Jr, Zbilut JP (1994) Dynamical assessment of physiological systems and states using recurrence plot strategies. J Appl Physiol 76(2):965–973
Yan L, Ren L, He XH, Lu SY, Guo H, Wu T (2020) Strong wind characteristics and buffeting response of a cable-stayed bridge under construction. Sensors 20:1228
Yang H (2011) Multiscale recurrence quantification analysis of spatial cardiac vectorcardiogram signals. ITBE 58(2):339–347
Zhang YM (2019) Experimental determination of aerodynamic admittance functions of a truss girder. School of Civil Engineering, Central South Univerisity, Changsha
Zou YF, Lei X, Yan L, He XH, Nie M, Xie WP, Luo XY (2020) Full-scale measurements of wind structure and dynamic behaviour of a transmission tower during a typhoon. Struct Infrastruct E 16(5):820–830

Publisher's Note